

## RESPONSE TO REVIEWER 1 COMMENTS

Ann. Geophys. Discuss.,  
<https://doi.org/10.5194/angeo-2018-35-RC1>, 2018  
© Author(s) 2018. This work is distributed under  
the Creative Commons Attribution 4.0 License.

MANUSCRIPT TITLE: **Solar Eclipse-Induced perturbations at mid-latitude during the 21 August 2017 event**

### GENERAL RESPONSE

We thank the reviewer for the useful and supportive corrections. We believe that all suggestions made have been considered accordingly in this revised edition of the manuscript. Major corrections have been effected accordingly, and are highlighted (colour red) in the manuscript text. We have modified the manuscript accordingly, and the detailed corrections are listed below point by point:

(Author (shown to authors):

### Major concerns:

#### **Comment 1**

- This manuscript attempts to provide a discussion related to the observed solar eclipse induced perturbations at the mid-latitude during the 21 August 2017. Although long description of this event and conclusions reached are supported by data analysis, the obvious question is what is really new in author's results and findings which have not already been reviled in the large number of the reference papers.

#### **Response to Comment 1**

- ✓ The new findings of this present work have been given in full detail in the body text (line 294 - 300) and thus summarized in the abstract (see line 18 – 26). Moreover, the study of the circumstances of solar eclipse at the topside ionosphere and its plasma distribution mechanisms using the bottomside parameters, scale height and the F2-layer parameters makes it significantly different from previous studies (see line 52 – 56).

#### **Comment 2**

- PP 39-42: In the context of the sentence “Different physical mechanisms (e.g. neutral wind, thermospheric composition, diffusion process etc.) that explain the distribution of plasma at the different ionospheric layers are well established”, the subsequent sentence “However, these mechanisms do compete with themselves in explaining other layers, especially for the topmost F2 layers”, is confusing. Particularly, who are “other layers” and where is “topmost” F2 layer?

#### **Response to Comment 2**

- ✓ The statement has been rewritten (now in line 36-39)

#### **Comment 3**

- PP46: “However”, should be deleted, and star the sentence simple - At equatorial and low-latitudes...

#### **Response to Comment 3**

- ✓ The “However” has been deleted and the correction has been made (see line 43)

#### **Comment 4**

- PP73: foF2 is an ionospheric characteristic not an ionospheric parameter

#### **Response to Comment 4**

- ✓ Thank you for this observation, the correction has been effected (see lines 72-73)

#### **Comment 5**

- PP272-273: The sentence “This paper presents the induced perturbation of solar eclipse of 21 August 2017 on the ionospheric F parameters and their behaviour in predicting one another at mid-latitude” is not clear to me

because I could not understand who is predicting what and where are the results of that prediction. See also the first sentence in Abstract and PP28.

**Response to comment 5**

- ✓ This sentence has been clarified both in the text and the abstract (see line 13-14 and line 275)

**Comment 6**

- PP276-277: There is not such name as “the F layer ionosphere”. As authors know very well, there are F1 and F2 layers or F region of the Earth’s ionosphere. See also PP281.

**Response to Comment 6**

- ✓ Thank you for this observation. This has been corrected in the text.

**Comment 7**

- Most importantly for the essence of the paper the last paragraph 252-267 is completely irrelevant. Furthermore, the IRI model is not generated to capture the conditions of the ionosphere during solar eclipse. See also PP285-287 as well as the last sentence in Abstract.

**Response to comment 7**

- ✓ This aspect has been completely removed from the manuscript as suggested.

**Comment 8**

- Although I am not a native English speaker, I feel free to suggest another careful proofread to avoid some minor typo and language errors. For example: PP80: NmF2 and hmF2- non italic; PP:84 NmF2, hmF2 – italic. See also a few more cases in the text; PP:214:  $(NmF2e - NmF2c)/NmF2c \times 100$  should be  $100 \times (NmF2e - NmF2c)/NmF2c$

**Response to Comment 8**

- ✓ Careful proofread of the manuscript has been carried out and all the language and typographical errors were corrected. For example: PP80 and PP84; NmF2 and hmF2 are now italicized (now in line 79 and 80). The text in PP214(Line 221) has been corrected accordingly.

Best regards,

ADEKOYA, B. J.  
For the Authors

## RESPONSE TO REVIEWER 2 COMMENTS

Ann. Geophys. Discuss.,  
<https://doi.org/10.5194/angeo-2018-35-RC1>, 2018  
© Author(s) 2018. This work is distributed under  
the Creative Commons Attribution 4.0 License.

MANUSCRIPT TITLE: **Solar Eclipse-Induced perturbations at mid-latitude during the 21 August 2017 event**

### GENERAL RESPONSE

We thank the reviewer for the useful and supportive corrections. We believe that all suggestions made have been considered accordingly in this revised edition of the manuscript. Major corrections have been effected accordingly, and are highlighted (colour red) in the manuscript text. We have modified the manuscript accordingly, and the detailed corrections are listed below point by point:

#### Major concerns:

##### *Comment 1*

- Line 15, please give a brief introduction to “GIRO database”, or at least give the full name of GIRO, otherwise it is difficult to know what kind of ionospheric parameters are used in your research

##### Response to Comment 1

- ✓ The GIRO means Global Ionospheric Radio Observatory database. This has been corrected in the manuscript (see page 1, line 15).

##### *Comment 2*

- Line 15, it is weird to use “percentage obscuration”. In my opinion, the percentage of obscuration or the obscuration percentage is better. Similar to Line 211 and Line 213, there are “percentage concentration of the components” and “percentage deviation”

##### Response to Comment 2

- ✓ The corrections have been effected now in lines 15 and 213

##### *Comment 3*

- Line 22, “Need for IRI model to capture eclipse caused perturbation”, it is not a complete sentence. Further, line 255-267, the authors said “IRI model doesn’t capture the conditions of the ionosphere during solar eclipse”, but didn’t show any figure or table to support this judge. And I don’t think IRI is a good tool to study ionospheric variations during solar eclipse

##### Response to Comment 3

- ✓ All IRI related statements in the manuscript have been deleted as suggested by Reviewer 1.

##### *Comment 4*

- Line 78-79, the authors said “The control day value is the mean of the values obtained on respective days ...” Specifically, which days did you choose as the control day? Was there geomagnetic storms in that period of time? Did you get the mean of the values by weighting?

##### Response to Comment 4

- ✓ The control day value is the average value of the two days before/after the eclipse day (i.e. 6, 12, 24 and 27). These reference days were chosen such that they have similar geomagnetic, interplanetary and solar properties with the eclipse day. The daily average value of the reference days and eclipse day for interplanetary index ( $A_p$  and  $\Sigma K_p$ ), and solar flux unit index (F10.7) ranges 8 – 12 nT for  $A_p$ , 20 – 27 nT for  $\Sigma K_p$  and 75.6 – 89.1 sfu (1 solar flux unit (sfu) =  $10^{-22}$  Wm<sup>-2</sup> Hz<sup>-1</sup>) for F10.7, indicating that geomagnetic and solar activities of these days is unsettled (see Adekoya et al., 2015 for classification of the activities). This is because under the same classifications, the effect of eclipse in the ionosphere is expected to be noticed when compared with the control day. The calculated daily average of summation  $K_p$ ,  $A_p$  and solar flux indices was obtained from the National Space Science data

Centres (NSSDC's) OMNI database <https://omniweb.gsfc.nasa.gov/>. This point has been included in the manuscript (see line 79 - 87)

**Comment 5**

- Line 241-242, the authors said “The only exception ... at Millstone... H versus B0 ...” however, it is clear that R is also low for the two figures of IDAHO.

**Response to comment 5**

- ✓ Thank you for the observation. The statement has been corrected accordingly (see line 262-264).

**Comment 6**

- Figures 1 and 2, for hmF2, scale height, bottomside, the variations of them are not very clear, especially at the stations of Eglin AFB, Boulder and Millstone Hill. I mean the noise is too large to get the valuable information. So it is a little far-fetched to draw your conclusion in “3 Result and Discussion”.

**Response to Comment 6**

- ✓ After critical observation of the said figures panels, the authors observed that there are no noise in the variations of the parameters during the eclipse window, rather the effect of eclipse was noted in comparison with the control day. Moreover, the digital ionosonde data used were from GIRO, which have minimal/negligible level of noise in the data records (see Reinisch and Galkin 2011; Reinisch et al., 2018). In addition, the reference days were chosen (as explained in Response to Comment 4) in a way that the data are not contaminated by noise, if there is any.

**Comment 7**

- Line 273-276, as the authors said, “ionospheric F2 parameters (NmF2 and hmF2), the bottomside profile thickness (B0) and shape (B1) parameters of electron density and the plasma scale height (H), which are not often used for eclipse study”, so have you considered that why these parameters are seldom used in eclipse study? I guess that is because the useful information is probably covered by the noise, especially for such parameters as hmF2, B0, B1 and H

**Response to comment 7**

- ✓ The use of the parameters in this study is a novel way of observing the ionospheric behavior at lower and topside ionosphere during solar eclipse, and as explained in Response to Comment 6, it is not associated with noise.

**Comment 8**

- Figure 3, how did you get this figure? I mean, for a certain electron density profile, there is only one NmF2 and hmF2. You know, NmF2 is F2 layer peak electron density and hmF2 is F2-layer peak density height. But in figure 3, it is very confusing that DNmF2 is varying with the change of Dhmf2. I guess you mean Ne and corresponding height. Maybe my understanding is wrong, Please explain this further for helping readers understand this clearly.

**Response to Comment 8**

- ✓ The clarification of Figure 3 has been explained to aid the readers' curiosity and understanding in line 221-255 and under figure caption in line 445 – 450.

**Comment 9**

- In abstract and conclusion, the authors said “predicting one another”. However, in the body of this manuscript, I didn't find which parameter is predicted. More importantly, the correlation between these parameters is not strong enough to predict each other. So it is not proper to judge that “Hence their relationship in predicting one another is established” If the authors want to prove that these parameters are predictable, they should provide some supporting figures or tables, instead of a very indiscreet sentence.

**Response to comment 9**

- ✓ We agree with your submission, and in line with the other reviewer's suggestion, we have deleted appropriately and the sentences have been rewritten both in the abstract and conclusion (see line 13-14 and line 275)

Best regards,  
ADEKOYA, B. J. (For the Authors)

# SOLAR ECLIPSE-INDUCED PERTURBATIONS AT MID-LATITUDE DURING THE 21 AUGUST 2017 EVENT

Bolarinwa J. Adekoya<sup>1</sup>, Babatunde O. Adebisin<sup>2</sup>, Timothy W. David<sup>1</sup>, Stephen O. Ikubanni<sup>2</sup>, and  
Shola J. Adebisi<sup>2</sup>

<sup>1</sup>Department of Physics, Olabisi Onabanjo University, P.M.B. 2002, Ago Iwoye, Nigeria

<sup>2</sup>Space Weather Group, Department of Physical Sciences, Landmark University, P.M.B 1001, Omu-Aran,  
Kwara State, Nigeria.

Correspondence to: Bolarinwa J. Adekoya ([adekoyabolrinwa@yahoo.com](mailto:adekoyabolrinwa@yahoo.com); [adekoya.bolarinwa@oouagoiwoye.edu.ng](mailto:adekoya.bolarinwa@oouagoiwoye.edu.ng))

## Abstract

A study of the response of some ionospheric parameters and their relationship in describing the behaviour of ionospheric mechanisms during the solar eclipse of 21 August 2017 is presented. Mid-latitude stations located along the eclipse path and with data availability on the Global Ionospheric radio Observatory (GIRO) database were selected. The percentage of obscuration at these stations range between 63-100%. Decrease in electron density during the eclipse is attributed to reduction in solar radiation and natural gas heating. The maximum magnitude of the eclipse coincided with  $hmF2$  increase and with a lagged maximum decrease in  $NmF2$  consistently at the stations investigated. The results revealed that the horizontal neutral wind flow is as a consequence of the changes in the thermospheric and diffusion processes. The unusual increase/decrease in the shape/thickness parameters during the eclipse period relative to the control days points to the perturbation caused by the solar eclipse. The relationship of the bottomside ionosphere and the F2 layer parameters with respect to the scale height are shown in the present work as viable parameters for probing the topside ionosphere during eclipse. Furthermore, this study shows that in addition to traditional ways of analysing the thermospheric composition and neutral wind flow, proper relation of standardized  $NmF2$  and  $hmF2$  can be conveniently used to describe the mechanisms.

**Keywords:** solar eclipse; solar radiation; bottomside profile parameters;  $NmF2$  and  $hmF2$ ; Topside ionosphere; GIRO database.

## 1 Introduction

Solar eclipse provides opportunity to study the causes of drastic changes in the atmosphere arising from reduction in solar radiation and plasma flux. The atmosphere responded to these changes by modifying the electrodynamic processes and ionization supply of its species to the nighttime-like characteristics during the daytime. Different physical mechanisms (e.g. neutral wind, thermospheric composition, diffusion process etc.) that explain the distribution of plasma at the different ionospheric layers are well established.

38 However, these mechanisms do compete with themselves in explaining the ionosphere, especially the  
39 topside ionosphere (see Gulyaeva, 2011).

40

41 At mid-latitudes, the effect of diffusion processes and its relationship with the thermospheric compositions  
42 has been extensively studied during episodes of solar eclipse (Muller-Wodarg et al., 1998; Jakowski et al.,  
43 2008; Le et al., 2009; Wang et al., 2010; Chuo, 2013). At equatorial and low-latitude regions, the  $E \times B$   
44 plasma drift had been used to explain the circumstances of solar eclipse on transport processes (Adeniyi et  
45 al., 2007; Adekoya et al., 2015). Recently, attention has been drawn to the study of the topside ionosphere  
46 during an eclipse for improved prediction and modelling (Huba and Drob, 2017; Chrniak and Zakharenkova,  
47 2018). Reinisch et al., (2018) compared the modelled and measured studies of electron densities at the  
48 altitude range of about 150 - 400 km during the eclipse. They found that at lower altitude (at about 150 km)  
49 the modelled and the measured agreed well to the changes in the altitude profile of electron density  
50 compared to at higher altitudes. The authors however posited that it would be improved if the model  
51  $NmF2$  peak falls more slowly to better match the data. Consequently, the present study investigates the  
52 effects of solar eclipse of August 21, 2017 on the constituents of the ionosphere at mid-latitudes using  
53 some ionosonde data (bottomside parameters, scale height (H) estimated from the fitted  $\alpha$ -Chapman layer)  
54 which have not been given much attention in previous works especially in analysing solar eclipse effect.  
55 Using these parameters to analyse the circumstances of solar eclipse at the topside ionosphere and its  
56 plasma distribution mechanisms make this paper significantly different from previous studies. This, we  
57 intend to achieve by analysing the ionospheric parameters that controls the distribution of plasma at the  
58 topside and bottomside layers of the F2 region. To shed light on these analysis, section 2 highlights the data  
59 source, methodology, and path of the eclipse. The result and discussion were presented in section 3, while  
60 section 4 presents the summary and concluding remark of the result.

61

## 62 **2 Data source, methodology, and the path of the eclipse**

63 With regards to the eclipse of 21 August 2017, the totality of the eclipse is visible from within a narrow  
64 corridor that traverses the United States of America. However, in the surrounding areas, which include all  
65 of mainland United States and Canada, the eclipse was partial. More details of its path can be seen via  
66 NASA – Total solar eclipse of 2017 August 21 (<https://eclipse.gsfc.nasa.gov/>). From the footprint of the  
67 Moon's shadow as seen from some locations, the eclipse started from around 08:00 LT and ended around  
68 14:30 LT (not shown). The details on the local circumstances of the eclipse, the time of the first, mid and  
69 last contact of the eclipse over the ionosphere of the investigated stations were highlighted in table 1.  
70 More details on the total solar eclipse event and its partiality, the circumstances surrounding its  
71 progression and its magnitude of obscuration can be obtained through the link

72 [http://xjubier.free.fr/en/index\\_en.html](http://xjubier.free.fr/en/index_en.html). The ionospheric parameters data used for this study for the  
73 selected mid-latitude stations were obtained from the Global Ionospheric Radio Observatory (GIRO)  
74 networks (Reinisch and Galkin 2011) and manually validated. The parameters include the maximum  
75 electron density of the F2-layer ( $NmF2$ ,  $m^{-3}$ ), and its height ( $hmF2$ ,  $km$ ), the shape parameter ( $B1$ ), the  
76 thickness parameter ( $B0$ ), and the Chapman scale height ( $H$ ) of the F2 layer. The path of the eclipse  
77 informed the choice of stations.

78  $NmF2$  values for both the eclipse and control days were obtained from their corresponding critical  
79 frequencies ( $foF2$ ) using the expression:  $NmF2 = ((foF2)^2 / 80.5) e/m^3$ . The control day value is the average  
80 value of the two days before/after the eclipse day (i.e. 6, 12, 24 and 27). These reference days were chosen  
81 such that they have similar geomagnetic, interplanetary and solar properties with the eclipse day. The daily  
82 average value of control days and eclipse day interplanetary index ( $Ap$  and  $\Sigma Kp$ ), and solar flux unit index  
83 ( $F10.7$ ) ranges from 8 – 12 nT for  $Ap$ , 20 – 27 nT for  $\Sigma Kp$  and 75.6 – 89.1 sfu (1 solar flux unit (sfu) =  $10^{-22}$   
84  $Wm^{-2} Hz^{-1}$ ) for  $F10.7$ , indicating that geomagnetic and solar activities of these days is unsettled (see  
85 Adekoya et al., 2015 for classification of geomagnetic activity). The calculated daily average of summation  
86  $Kp$ ,  $Ap$  and solar flux indices was obtained from the National Space Science data Centres (NSSDC's) OMNI  
87 database <https://omniweb.gsfc.nasa.gov/>. The typical behaviour of the  $NmF2$  and  $hmF2$  on the eclipse day  
88 (i.e.  $NmF2e$  and  $hmF2e$ ) was compared with that of the control day ( $NmF2c$  and  $hmF2c$ ) to observe the  
89 changes brought by the short period of loss of photoionization in the ionosphere. This will measure the  
90 direct consequence of the solar radiation disruption (due to the eclipse) on the ionospheric chemical,  
91 transport and thermal processes in the F2 layer. The ionized layer depends majorly on three parameters,  
92 viz:  $NmF2$ ,  $hmF2$ , and the ionospheric scale height ( $H$ ). The  $H$  describes the constituents of the ionospheric  
93 plasma, which decreases with increasing altitude. It is estimated from the fitted  $\alpha$ -Chapman layer with a  
94 variable scale height,  $H(h)$ , to the measured bottomside profile  $N(h)$ , which then determined as the  
95 Chapman scale height at  $hmF2$  (i.e.  $H(hmF2) = H$ ) (Huang and Reinisch 2001; Reinisch and Huang 2001).  
96 Together with the information of  $NmF2$  and  $hmF2$ , the topside profile can be best represented, which is  
97 assumed to follow the  $\alpha$ -Chapman function (Huang and Reinisch 2001). Also,  $H$  provides a linkage between  
98 the bottomside ionosphere and the topside profiles of the F region (Liu et al., 2007).

99

100 However, Xu et al. (2013) and Gulyaeva (2011) related ionospheric F2 - layer scale height,  $H$  to the topside  
101 base scale height,  $Hsc$ , given by  $Hsc = hsc - hmF2 \approx 3 \times H$ . Where  $hsc$  is the height at which the electron  
102 density of the F2-layer falls by a factor of an exponent, at an upper limit of 400 km altitude (i.e.  $NmF2/e$ )  
103 (see Xu et al., 2013). That is, the region where electron density profile gradient is relatively low. Gulyaeva  
104 (2011) showed theoretically that  $Hsc$  increase over  $Hm$  by a factor of approximately three (3) and is a

105 consequence of the  $Ne/NmF2$  ratio ( $Ne$  – plasma density), which corresponds to  $H$  in the Chapman layer. At  
106 altitudes very close to  $hmF2$ , the ratio equals 0.832, while it is 0.368 at altitudes beyond the  $hmF2$ .  
107 Therefore, we adopted the definition of Gulyaeva (2011) for the topside base scale height as the region of  
108 the ionosphere between the F2-peak and 400 km altitude. Summarily, the topside based scale height  
109 ionosphere here is defined as the region between the F2 peak and  $hsc$  or  $3H$ . It is thus evident that  $H$  is a  
110 key and essential parameter in the continuity equation for deriving the production rate at different  
111 altitudes, a pointer to the F2 topside electron profiler, as well as a good parameter for evaluating the  
112 transport term (Yonezawa, 1966; Huang and Reinisch, 2001; Reinisch and Huang, 2001; Belehaki et al.,  
113 2006; Reinisch et al., 2004). Consequently, the parameter  $H$  can be used as a proxy for observation relating  
114 to the topmost side electron density profile. Furthermore, the division of the topsides and the bottomside  
115 ionosphere may be related to the difference in the effective physical mechanisms in the regions. Hence, the  
116 bottomside parameters  $B1$  and  $B0$  of the ionosphere, as presented in this work, helped in examining the  
117 perturbation of solar eclipse in the bottomside ionospheric F2 layer.

118

### 119 **3 Result and Discussion**

120 This section presents the temporal evolution of the maximum electron density ( $NmF2$ ), and its  
121 corresponding height ( $hmF2$ ) over the ionosphere at the selected mid-latitude stations along the path of  
122 solar eclipse of 21 August 2017. The control day variation relative to the eclipse day is also presented.  
123 Figure 1 presents the variation of maximum electron density and the corresponding peak height, during  
124 both the eclipse and control days. Figure 2 depicts the variation of scale height and the bottomside  
125 parameters ( $B0$  and  $B1$ ) due to the eclipse by superposing plots for both the eclipse and control days.  
126 Analysis of these parameters during an eclipse event may help in the modelling of the ionospheric profiles  
127 (the topsides and bottomside electron density distribution profile) during the short nighttime-like period of  
128 the day. Figure 1a presents the  $NmF2$  and  $hmF2$  variations during the eclipse event and the control day  
129 over Austin; having an obscuration magnitude of 65.93% around the daytime period. The effect of the  
130 disruption of solar radiation was evident as the  $NmF2$  started decreasing at the first contact of the eclipse  
131 in Fig. 1ai. The start time or first contact, the maximum magnitude period and the end time or the last  
132 contact of the eclipse are marked with the vertical lines S, M and E respectively. The decrement in  $NmF2$   
133 during the eclipse phase was due to reduction in the ionization. This reduction caused changes in the  
134 photochemical and transport process of the atmosphere during the daytime, thus exhibiting nighttime  
135 characteristics. It should be noted that the maximum decrease in  $NmF2$  did not coincide with the maximum  
136 magnitude of the eclipse obscuration, rather with a time lag of few minutes. This lag period fell within the  
137 relaxation period over Austin ionosphere, with  $NmF2$  and  $hmF2$  simultaneously attaining their peak



138 magnitudes. Hence, the ionosphere returned to its pre-eclipse state. Contrary to the decrease in the *NmF2*  
139 amplitude, the *hmF2* increased at the total obscuration of the eclipse window.

140

141 The ionosphere over Eglin AFB, Boulder, Point Arguello, Millstone Hill and Idaho National Lab, did not show  
142 any contrary variation to that observed at Austin during the eclipse event. The decrease and increase in  
143 *NmF2* and *hmF2* after the maximum magnitude was simultaneous. The only exception was that the local  
144 time at which each station observed the effects were different. Their obscuration percentage ranged from  
145 62.5 – 100%. This did not cause any significant change in the way they responded to the reduction in solar  
146 heating. The ionosphere over Idaho National Lab experienced the totality of the eclipse with 100 %  
147 magnitude, the *hmF2* was observed to increase few minutes before the maximum magnitude of the  
148 obscuration. However, other stations responded differently, their *hmF2* peak enhancement was observed  
149 after the maximum obscuration. All these observations may be linked with the fact that the level of  
150 minimum rate of electron production does not necessarily coincide with peak electron density of the  
151 molecular gases formed. This is because the electron concentration depends on the loss rate by dissociative  
152 recombination too.

153

154 At mid-latitudes, the ionospheric F2 plasma distribution is controlled by diffusion processes (Rishbeth  
155 1968). There are two basic mechanisms that define the diffusion process during an eclipse: First is the  
156 coolness brought by the partial removal of photoionization (Müller-Wodarg et al., 1998), which is believed  
157 to be the originator of the downward diffusion process, and the atmospheric expansion due to the gradual  
158 increase in the temperature after the totality. The downward diffusion process was related to the increase  
159 in the molecular gas ( $N_2$ ) concentration during the cooling process. However, the aftermath of the coolness  
160 was related to the upward diffusion process. These mechanisms were proxy to the electron density  
161 distribution during the eclipse window. Our analysis suggests that the observed decrease in *NmF2* is due to  
162 the downward diffusion flux of the plasma while the increase that followed is by upward diffusion (e.g. Le  
163 et al., 2009; Adekoya and Chukwuma 2016). Several works on eclipse (Müller-Wodarg et al., 1998;  
164 Grigorenko et al., 2008; Adekoya and Chukwuma 2016; Hoque et al., 2016) have shown that it was not just  
165 the electron density that is being affected during an eclipse window, but the thermospheric wind as well,  
166 since the thermospheric wind emanating from the ratio of gas species is related to the variation in electron  
167 density. It has been observed that the increase in the mean molecular gas of thermospheric composition  
168 decreases the electron density and vice versa. Le et al. (2010) related the trough of electron density  
169 distribution during the eclipse phases to the contraction/compression and expansion of the atmosphere  
170 brought by the decrease and increase in temperature; leading to the downward drift of the plasma during  
171 the eclipse window. Chukwuma and Adekoya (2016) attributed the decrease in the electron temperature to

172 the downward vertical transport process and the decrease in the cooling process to the upward vertical  
173 transport process.

174

175 Figure 2 describes  $H$ ,  $B1$  and  $B0$  in three columns respectively for all six stations. It was observed from the  
176 plots that the minimum decrease in  $NmF2$  amplitude corresponds to increase in  $H$  at all stations; implying  
177 the upward lifting of the topside electron to the region of higher altitude at the eclipse window. Hence, the  
178 scale height variation highlights the decrease in electron production and the vertical distance through  
179 which the pressure gradient falls at the topside during the eclipse activity. The observation illustrates the  
180 mutual relationship between the  $NmF2$  and  $H$ , which may aid in extrapolating the topside ionospheric  
181 profile (Gulyaeva, 2011). In essence, scale height changes observed during the eclipse window can be used  
182 to explain the pressure gradient, electron density distribution and transport processes. In this sense, the  
183 diffusion coefficients are expressed as ratio of determinants (determinant here refers to the concentration  
184 of species ( $[O]$  and  $[N_2]$ )), with the size of the determinants depending upon both the number of species in  
185 the gas mixture and the level of approximation. Therefore, the increase (decrease) in the scale height can  
186 be used as a proxy for downward (upward) diffusion process at the topside ionosphere. Consequently, the  
187 thermospheric wind, which causes plasma distribution in the topside ionosphere, is induced by solar  
188 radiation. Moreover, the significant changes observed in the scale height variation during the eclipse  
189 window also indicated that transport processes are affected as they are temperature dependent.  
190 Therefore, changes in the thermospheric compositions due to the solar eclipse at the topside layer will  
191 affect the density profiles of the ionosphere (Müller-Wodarg et al., 1998).

192

193 It is noteworthy that the increase (decrease) in the scale height decreases (increases) the electron density  
194 during the eclipse window. The sensitivity of electron density to temperature at the topside directly affects  
195 the electron density profile (e.g. Wang et al., 2010); as cooling due to decrease in temperature results in  
196 decrease in the electron density via reduced ionization. This indicates that the decrease (increase) in  
197 electron temperature at the topside ionosphere causes the increase (decrease) in the scale height, which is  
198 related to the diffusion and transport processes and subsequently affect the pressure gradient of the  
199 plasma. From plots of  $H$  (fig. 2) and  $NmF2$  (fig. 1), it was observed that the minimum decrease in  $NmF2$   
200 corresponded with peak increase in scale height. This imply that the topside ionosphere is more sensitive  
201 (than the bottomside) to any change in the solar radiation. Thus, the pressure gradients can be analysed in  
202 terms of either the scale height or electron density.

203

204 From column 2 and 3 of Figure 2, we observed that the measured shape ( $B1$ ) and thickness ( $B0$ ) parameters  
205 of the ionosphere over these stations exhibit significant variations during the eclipse event.  $B1$  responded

206 with a decrease at the first contact of the eclipse compared to the control day. This behaviour differs from  
207 that of the *BO* observation. *BO* parameter from the first contact increases and reached the maximum peak  
208 few minutes after the maximum obscuration magnitude, which coincided with the minimum decrease in  
209 *BO*. Generally, the pattern of the day to day variation of the bottomside parameters is the average  
210 morphology, but the increase in the *BO* and the decrease in the *B1* parameters during the eclipse period  
211 compared to the control day was a notable one and can be related to the perturbation caused by the solar  
212 eclipse. During the eclipse, the solar radiation was lost; trapped atomic ions  $O^+$  was converted into  
213 molecular ion ( $NO^+$  and  $O_2^+$ ) by charge transfer, owing to the sufficient concentration of molecular gasses  
214 ( $N_2$  and  $O_2$ ) (Rishbeth, 1988). The height of the ionospheric slab indeed increased with reduced width,  
215 which is attributable to compression due to loss of solar heating.

216

217 The behaviour of the ionosphere can be explained during solar eclipse with any of the components that  
218 constitute the topside and the bottomside ionosphere and can be looked at, from the angle of the  
219 **percentage of concentration** of the components. In this regard, the **percentage of deviations** of *NmF2*  
220 (*DNmF2*) and *hmF2* (*DhmF2*) during the eclipse day away from the control day were plotted in Figure 3. This  
221 is done to describe the contribution of the thermospheric wind and compositions. **Although observing the**  
222 **variation of *NmF2* and *hmF2* alone can be used for observing the changes in the behaviour of the**  
223 **thermospheric compositions and wind flow, if properly analysed, but it is more convenient to describe**  
224 **these mechanisms by standardizing the original variables used during the event. The normalization effort**  
225 **(with the use of *DNmF2* and *DhmF2*) presents the original variation of *NmF2* and *hmF2* onto directions**  
226 **which maximize the variance. Consequently, the result can be used for analyses of any mechanisms that**  
227 **drive the ionospheric plasma, if properly related.**

228

229 The percentage deviation in Figure 3 was defined as the ratio of  $((NmF2e - NmF2c)/NmF2c) \times 100$ . The  
230 same relation is defined for the *hmF2* parameter. As earlier pointed out, during eclipse period, neutral  
231 composition becomes the dominant chemical process arising from diffusion activities. The increase in the  
232 neutral composition leads to the increase in the molecular gas concentration and compete with diffusion  
233 process. Hence the percentage deviation in Fig. 3 discusses the neutral composition changes and delineate  
234 how these changes may affect the electron densities as well as its profiles in the atmosphere during the  
235 eclipse. The respective maximum and minimum peak response of the percentage deviation is attributed to  
236 the enhancement and depletion of *DNmF2*. One sees from the plots that the percentage deviation started  
237 increasing at the first contact of the eclipse (the dash vertical line) and reached the maximum, appearing  
238 few minutes after the maximum magnitude of the eclipse was obtained. This behaviour is similar to the  
239 conditions of the neutral compositions during the eclipse event reported by Muller-Wodarg et al. (1998).

240

241 Another important process observed in this study is the neutral wind flow effect. To identify the direction  
242 of the wind, the  $DNmF2$  colour legend in the contour plots was used in Figure 3. The negative values  
243 represent a westward wind contribution and the positive values is for the eastward wind. Looking at the  
244 marked eclipse region in the figure, it would be seen that the  $DNmF2$  started decreasing from the first  
245 contact of the eclipse and maximized few minutes after the totality mark and started increasing again. It  
246 has been established that at daytime, the peak height of the plasma will be reduced due to lost in  
247 recombination; but at nighttime, equatorward neutral wind drives the F2-layer plasma to higher altitudes  
248 where ion loss rate is slower. The behaviour of the F2 plasma during solar eclipse cannot be completely  
249 related to the nighttime period due to the fact that all the processes controlling the nighttime variation are  
250 not completely actualised but can be related to partial nighttime/sunset period (see Adekoya et al., 2015).  
251 Thus, the slight increase in the peak height and equatorward neutral wind flow is the driver during the solar  
252 eclipse phase. The neutral wind acts jointly with the plasma flows from the topside ionosphere, resulting in  
253 F2 region plasma density variation. Therefore, the westward/eastward neutral wind flow was related to the  
254 depletion/enhancement in the deviation, which was clearly shown in the marked eclipse region of the  
255 figure. The plot in Figure 3 had established the ionospheric dynamics of diffusion processes, neutral  
256 compositions and the flow of neutral wind caused by the eclipse perturbation, which can invariably reduce  
257 the effectiveness and reliability of radio wave propagation.

258

259 Relative to the mutual relationship between the topside and bottomside ionosphere, we considered the  
260 linear correlation coefficient ( $R$ ) of  $H$  versus  $hmF2$  and  $H$  versus  $BO$  during the eclipse window, Figure 4.  $R$   
261 ranges from (0.52-0.92) for  $H/hmF2$  relationship, and 0.37-0.92 for the  $H/BO$  connection. This good linear  
262 agreement revealed the dependence of  $hmF2$  and  $BO$  on the scale height. The only exception where low  
263 correlation was observed was at Idaho (0.47) and Millstone (0.37) with respect to the  $H$  versus  $BO$   
264 relationship. Apart from revealing the dependence between the parameters, the relationship may also  
265 provide a convenient way for modelling the topside profile from the knowledge of the bottomside  
266 parameter,  $BO$ , during the eclipse period. Also, the strong correlation between  $hmF2$  and  $H$  indicates that  
267 there may be some inter-related physical mechanisms controlling the behaviour of the plasma at the  
268 topside ionosphere. That is  $hmF2$  strongly depend on the neutral wind flow and explain the state of  
269 thermospheric composition (Liu et al., 2006; Fisher et al., 2015). Since all these parameters competes  
270 during the eclipse, one can argue that with the accessibility of one, in place of the other (as a consequence  
271 of their relationship), the prediction and modelling of the ionosphere can be conveniently achieved.

272

#### 273 **4 Conclusions**

274 This paper presents the induced perturbation of solar eclipse of 21 August 2017 on the ionospheric F  
275 parameters and **how they describe the mechanisms of the ionosphere at mid-latitude**. The perturbation  
276 effects and dynamics during a solar eclipse episode using ionospheric F2 parameters ( $NmF2$  and  $hmF2$ ), the  
277 bottomside profile thickness ( $B0$ ) and shape ( $B1$ ) parameters of electron density and the plasma scale  
278 height (H), which are not often used for eclipse study, were investigated. These parameters represent the  
279 state of the **F-region** ionosphere. The changes observed during the eclipse phase is related to the reduction  
280 in solar radiation and natural gas heating. The  $NmF2$  minimum was attained at ~30 minutes after the  
281 totality of the eclipse when it decreases to about 65% of its control day. This decrease in  $NmF2$  was uplifted  
282 to the higher altitude compared to the non-eclipse day. The thickness and shape parameters which are  
283 often limited to the bottomside **F-region** were seen as viable parameters for probing the topside  
284 ionosphere, relative to the scale height during the eclipse. Hence their **relationship in describe one another**  
285 is established. Implication is that eclipse-caused perturbation could have been better explained using some  
286 ionosonde parameters. The changes in the neutral wind flow, thermospheric compositions and diffusion  
287 processes found their explanation in the behaviour of the F region plasma during eclipse. **In addition, it can**  
288 **be concluded that the behaviour of  $DNmF2$  and  $DhmF2$  during eclipse can be conveniently used to describe**  
289 **the mechanisms of thermospheric composition and wind flow.**

#### 291 **Acknowledgements**

292 We acknowledge use of global ionospheric Radio Observatory data provided by ULMCAR  
293 (<http://ulcar.uml.edu/DIDBase/>) and the World Data Center for Geomagnetism, Kyoto  
294 (<http://wdc.kugi.kyoto-u.ac.jp/index.html>) for geomagnetic activity data. We thank the management team  
295 of the national Aeronautics and Space Administration (NASA) service (<http://eclipse.gsfc.nasa.gov>) and  
296 [http://xjubier.free.fr/en/site\\_pages/SolarEclipseCalc\\_Diagram.html](http://xjubier.free.fr/en/site_pages/SolarEclipseCalc_Diagram.html) for progression and eclipse local  
297 circumstances information. **The authors thank Professor Ljiljana R, Cander and the anonymous reviewer for**  
298 **their constructive corrections and suggestions that tremendously improved the structure and quality of the**  
299 **paper.**

#### 301 **References**

- 302 Adeniyi, J. O., Radicella, S. M., Adimula, I. A., Willoughby, A. A., Oladipo, O. A., and Olawepo, O.: Signature  
303 of the 29 March 2006 eclipse on the ionosphere over an equatorial station, J. Geophys. Res, 112 (A6),  
304 A06314. <http://dx.doi.org/10.1029/2006JA012197>, 2007.
- 305
- 306 Adekoya, B. J., Chukwuma, V. U., and Reinisch, B. W.: Ionospheric vertical plasma drift and electron density  
307 response during total solar eclipses at equatorial/low latitude, J. Geophys. Res, 120, 8066-8084.  
308 doi:10.1002/2015JA021557, 2015.
- 309
- 310 Adekoya, B. J., and Chukwuma, V. U.: Ionospheric F2 layer responses to total solar eclipses at low- and mid-  
311 latitude, J. Atmos. Sol. Terr. Phys., 138-139, 136-160. <http://dx.doi.org/10.1016/j.jastp.2016.01.006>, 2016.
- 312

313 Belehaki, A., Marinov, P., Kutiev, I., Jakowski, N., and Stankov, S.: Comparison of the topside ionosphere  
314 scale height determined by topside sounders model and bottomside digisonde profiles, *Adv. Space Res.*,  
315 <http://dx.doi.org/10.1016/j.asr.2005.09.015>, 2006.  
316

317 Cherniak, I., and Zakharenkova, I.: Ionospheric Total Electron Content response to the great American solar  
318 eclipse of 21 August 2017, *Geophys. Res. Lett.*, <http://dx.doi.org/10.1002/2017GL075989> , 2018.  
319

320 Chukwuma, V. U., and Adekoya, B. J.: The effects of March 20, 2015 solar eclipse on the F2 layer in the mid-  
321 latitude, *Advances in Space Research*, 58, 1720-1731. <http://dx.doi.org/10.1016/j.asr.2016.06.038> , 2016.  
322

323 Chuo, Y. J.: Ionospheric effects on the F region during the sunrise for the annular solar eclipse over Taiwan  
324 on 21 May 2012, *Ann. Geophys.*, 31, 1891-1898. doi:10.5194/angeo-31-1891-2013, 2013  
325

326 Fisher, D. J., Makela, J. J., Meriwether, J. W., Buriti, R. A., Benkhaldoun, Z., Kaab, M., and Lagheryeb, A.:  
327 Climatologies of nighttime thermospheric winds and temperatures from Fabry-Perot interferometer  
328 measurements: From solar minimum to solar maximum, *J. Geophys. Res.*, 120, 6679-6693,  
329 doi:10.1002/2015JA021170, 2015.  
330

331 Grigorenko, E. I., Lyashenko, M. V., and Chernogor, L. F.: Effects of the solar eclipse of March 29, 2006, in  
332 the ionosphere and atmosphere, *Geomagnetism and Aeronomy*, 48 (3), 337-351.  
333 <http://dx.doi.org/10.1134/S0016793208030092>, 2008.  
334

335 Gulyaeva T. L.: Storm time behaviour of topside scale height inferred from the ionosphere-plasmasphere  
336 model driven by the F2 layer peak and GPS-TEC observation, *Adv. Space Res.*, 47, 913-920.  
337 doi:10.1016/j.asr.2010.10.025, 2011.  
338

339 Hoque, M. M., Wenze, I. D., Jakowski, N., Gerzen, T., Berdermann, J., Wilken, V., Kriegel, M., Sato, H.,  
340 Borries, C., and Minkwitz, D.: Ionospheric response over Europe during the solar eclipse of March 20, 2015,  
341 *J. Space Weather Space Clim.*, 6 (A36). doi: 10.1051/swsc/2016032, 2016.  
342

343 Huba, J. D., and Drob, D.: SAMI3 prediction of the impact of the 21 August 2017 total solar eclipse on the  
344 ionosphere/plasmasphere system, *Geophys. Res. Lett.*, 44, 5928-5935.  
345 <http://dx.doi.org/10.1002/2017GL073549>, 2017.  
346

347 Huang, X. and B. W. Reinisch, B. W.: Vertical electron content from ionograms in real time, *Radio Sci.*, 36  
348 (2), 335 – 342, 2001.  
349

350 Jakowski, N., Stankov, S. M., Wilken, V., Borries, C., Altadill, D., Chum, J., Buresova, D., Boska, J., Sauli, P.,  
351 Hruska, F. and Cander, Lj. R.: Ionospheric behaviour over Europe during the solar eclipse of 3 October 2005,  
352 *J. Atmos. Sol. Terr. Phys.*, 70, 836-853. <http://dx.doi.org/10.1016/j.jastp.2007.02.016>, 2008.  
353

354 Le, H., Liu, L., Yue, X., Wan, W., and Ning, B.: Latitudinal dependence of the ionospheric response to solar  
355 eclipse, *J. Geophys. Res.*, 114, A07308. <http://dx.doi.org/10.1029/2009JA014072> , 2009.  
356

357 Le, H. Le, Liu, Libo, Ding, Feng, Ren, Zhipeng, Chen, Yiding, Wan, Weixing, Ning, Baiqi, Guirong, Xu, Wang,  
358 Min, Li, Guozhu, Xiong, Bo, Lianhuan, Hu: Observations and modeling of the ionospheric behaviors over the  
359 east Asia zone during the 22 July 2009 solar eclipse. *J. Geophys. Res.*, 115, A10313.  
360 <http://dx.doi.org/10.1029/2010JA015609>, 2010.  
361

362 Liu, L., Wan, W., and Ning B.: A study of the ionogram derived effective scale height around the ionospheric  
363 *hmF2*, Ann. Geophys., 24 (3), 851-860. [www.ann-geophys.net/24/851/2006/](http://www.ann-geophys.net/24/851/2006/), 2006.  
364

365 Liu, L., Le, H., Wan, W., Sulzer, M. P., Lei, J., and Zhang, M. -L.: An analysis of the scale heights in the lower  
366 topside ionosphere based on the Arecibo incoherent scatter radar measurements, J. Geophys. Res., 112,  
367 A06307, <http://dx.doi.org/10.1029/2007JA012250>, 2007.  
368

369 Müller-Wodarg, I. C. F., Aylward, A. D., and Lockwood, M.: Effects of a Mid-Latitude Solar Eclipse on the  
370 Thermosphere and Ionosphere - A Modelling Study, Geophys. Res. Lett., 25(20), 3787-3790, 1998.  
371

372 Reinisch, B. W., Dandenault, P. B., Galkin, I. A., Hamel, R., and Richards R. P.: Investigation of the electron  
373 density variation during the August 21, 2017 Solar Eclipse, Geophys. Res. Lett., doi:  
374 10.1002/2017GL076572, 2018.  
375

376 Reinisch, B. W. and Galkin, I. A.: Global Ionosphere Radio Observatory (GIRO), Earth Planets Space, 63 (4),  
377 377-381. <https://doi.org/10.5047/eps.2011.03.001>, 2011.  
378

379 Reinisch, B. W., Huang, X., Belehaki, A., Shi, J., Zhang, M., and Ilma, R.: Modeling the IRI topside profile  
380 using scale heights from ground-based ionosonde measurements, Adv. Space Res., 34 (9), 2026-2031.  
381 <https://doi.org/10.1016/j.asr.2004.06.012>, 2004.  
382

383 Reinisch, B. W., and Huang, X.: Deducing topside profiles and total electron content from bottomside  
384 ionograms, Adv. Space Res., 27 (1), 23-30. [https://doi.org/10.1016/S0273-1177\(00\)00136-8](https://doi.org/10.1016/S0273-1177(00)00136-8), 2001.  
385

386 Rishbeth, H.: Solar eclipses and ionospheric theory. Space Science Review, 8 (4), 543-554.  
387 <https://doi.org/10.1007/BF00175006>, 1968.  
388

389 Rishbeth, H.: Basic physics of the ionosphere: A tutorial review, Journal of Institute of The Electronics and  
390 Radio Engineers, 58 (6S), S207-S223. doi:10.1049/jiere.1988.0060, 1988.  
391

392 Xu, T. L., Jin, H. L., Xu, X., Guo, P. Wang, Y. B., Ping, J. S.: Statistical analysis of the ionospheric topside scale  
393 height based on COSMIC RO measurements, J. Atmos. Sol. Terr. Phys., 104, 29 – 38.  
394 <http://dx.doi.org/10.1016/j.jastp.2013.07.012>, 2013.  
395

396 Wang, X., Berthelier, J. J., and Lebreton, J. P.: Ionosphere variations at 700 km altitude observed by the  
397 DEMETER satellite during the 29 March 2006 solar eclipse, J. Geophys. Res., 115, A11312.  
398 <http://dx.doi.org/10.1029/2010JA015497>, 2010.  
399

400 Yonezawa, T.: Theory of formation of the ionosphere, Space Science Review, 5 (1), 3-56.  
401 <https://doi.org/10.1007/BF00179214>, 1966  
402

403  
404

405 **Table Caption**

406 **Table 1:** List of ionosonde station, geographic coordinate, eclipse progression time and percentage of  
407 maximum obscuration.

408 **Figure Captions**

409 **Figure 1:** Ionospheric  $NmF2$  and  $hmF2$  variations during the eclipse day (black continuous line) and the  
 410 control day (dash blue line). The three vertical lines represents the different phases of the eclipse (S - start  
 411 time of the initial phase, M - the period of the maximum magnitude of the eclipse, and E - the end time of  
 412 the recovery phase or the last contact of the eclipse progression).

413 **Figure 2:** The local time variation of the ionospheric scale height and the bottomside ( $BO$  and  $B1$ ). The other  
 414 features are the same as in Fig. 1.

415 **Figure 3:** Percentage deviation of  $NmF2$  ( $DNmF2$ ) and  $hmF2$  ( $DhmF2$ ) magnitudes during the 21 August  
 416 2017 eclipse phase.

417 **Figure 4:** Linear relationship of  $H$  versus  $hmF2$  and  $H$  versus  $BO$  during the eclipse of 21 August 2017  
 418 progression phase.

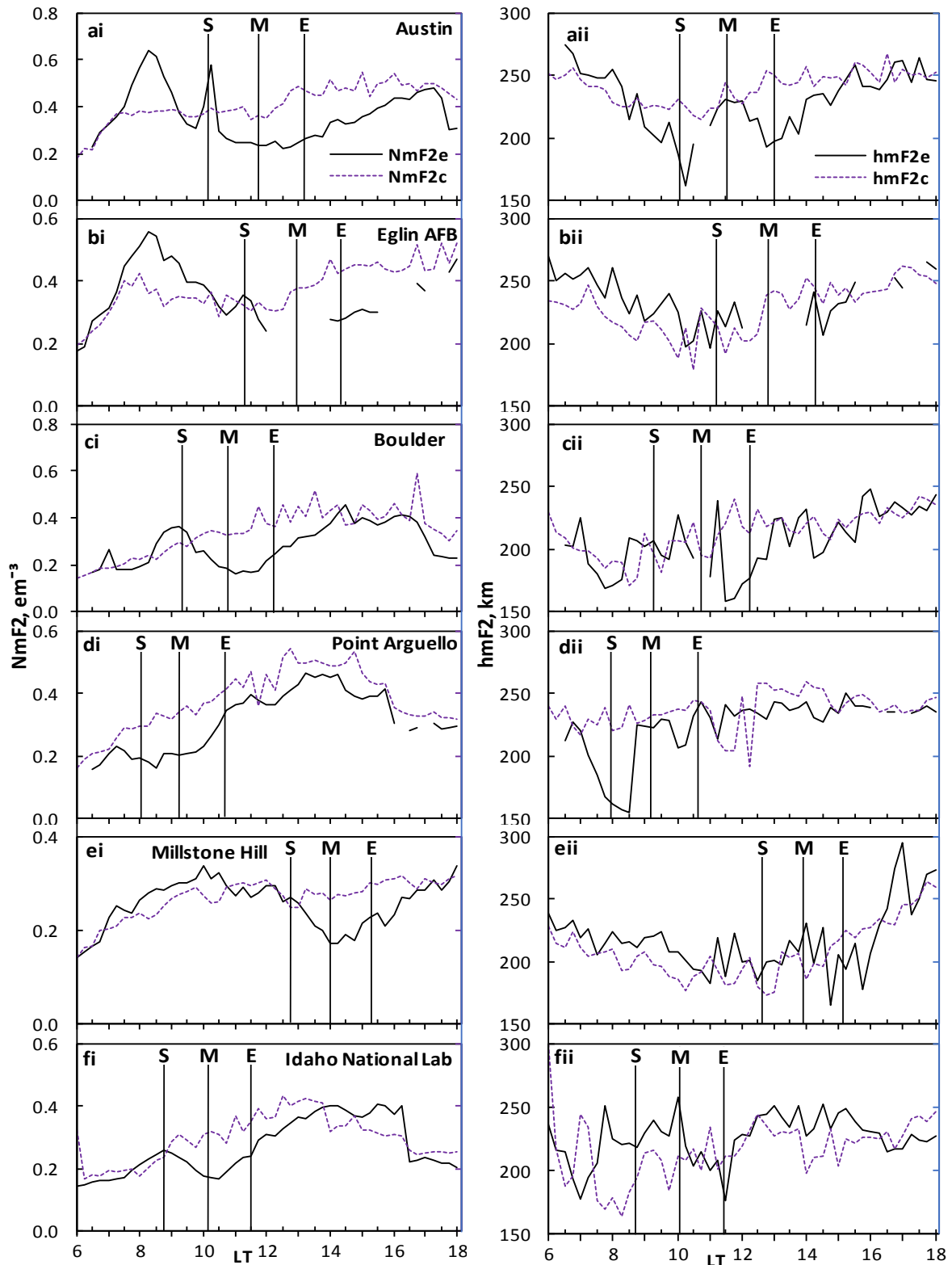
419  
 420  
 421  
 422  
 423  
 424  
 425  
 426  
 427  
 428  
 429

430 **Table 1:** List of ionosonde station, geographic coordinate, eclipse progression time and percentage of  
 431 maximum obscuration.

Station	GLat	GLong	Eclipse Start time (UT)	Eclipse Max Time (UT)	Eclipse End Time (UT)	% of max obscuration	UT to LT difference
AUSTIN	30.4	262.3	16:40:45.1	18:10:10.3	19:39:35.0	65.93	17:29.2
EGLIN AFB	30.5	273.5	17:04:41.1	18:37:07.6	20:03:47.7	83.322	18:13.8
POINT ARGUELLO	34.8	239.5	16:02:38.5	17:16:54.8	18:39:36.0	64.608	15:57.6
BOULDER	40	254.7	16:22:33.1	17:46:09.6	19:13:45.9	93.37	16:58.8
MILLSTONE HILL	42.6	288.5	17:27:28.1	18:45:52.5	19:58:38.3	62.533	19:13.8
IDAHO NATIONAL LAB	43.81	247.32	16:14:15.2	17:32:36.5	18:56:30.1	100	16:29.3

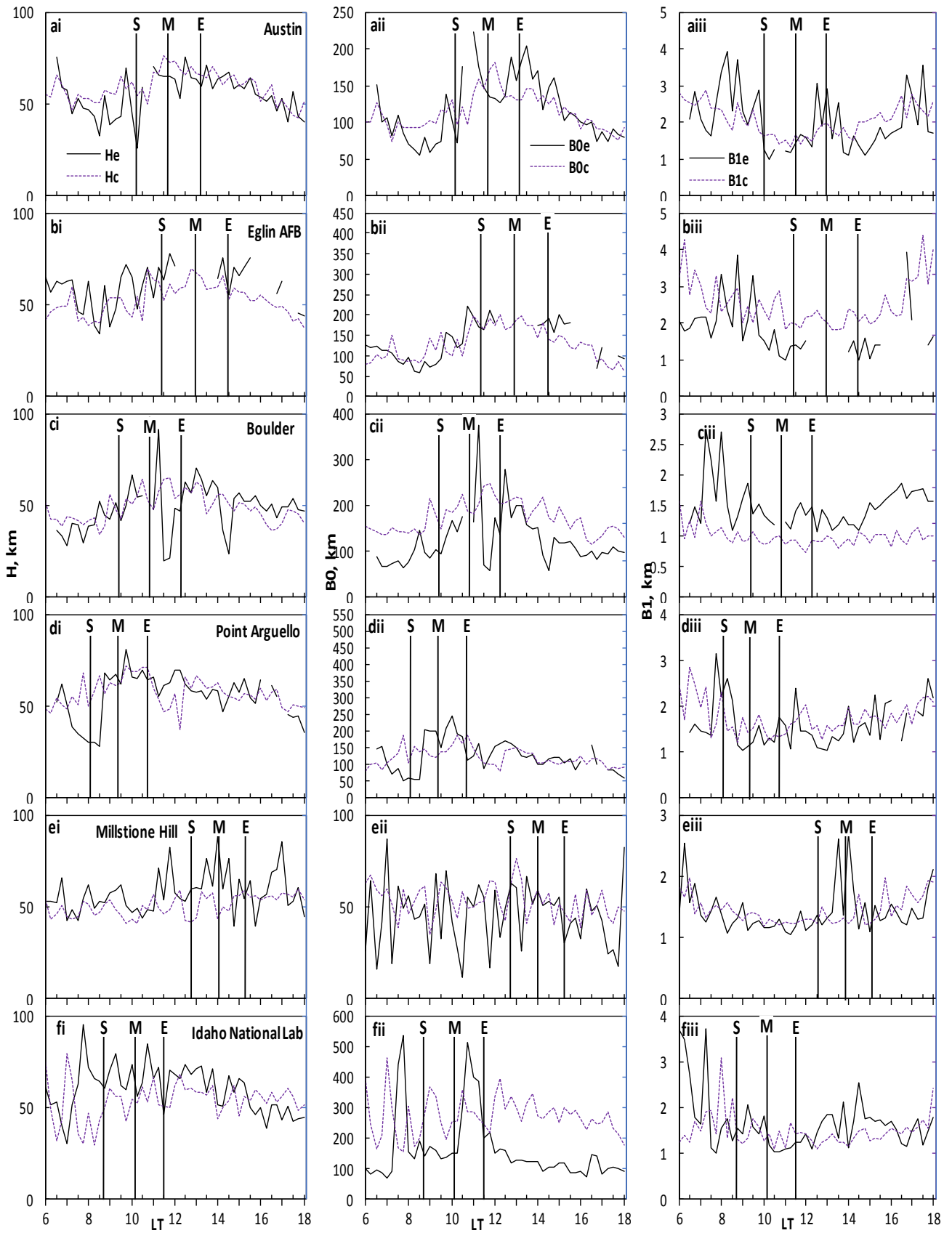
432  
 433  
 434  
 435





436

437 **Figure 1:** Ionospheric  $NmF2$  and  $hmF2$  variations during the eclipse day (black continuous line) and the  
 438 control day (dash blue line). The three vertical lines represents the different phases of the eclipse (S - start  
 439 time of the initial phase, M - the period of the maximum magnitude of the eclipse, and E - the end time of  
 440 the recovery phase or the last contact of the eclipse progression).

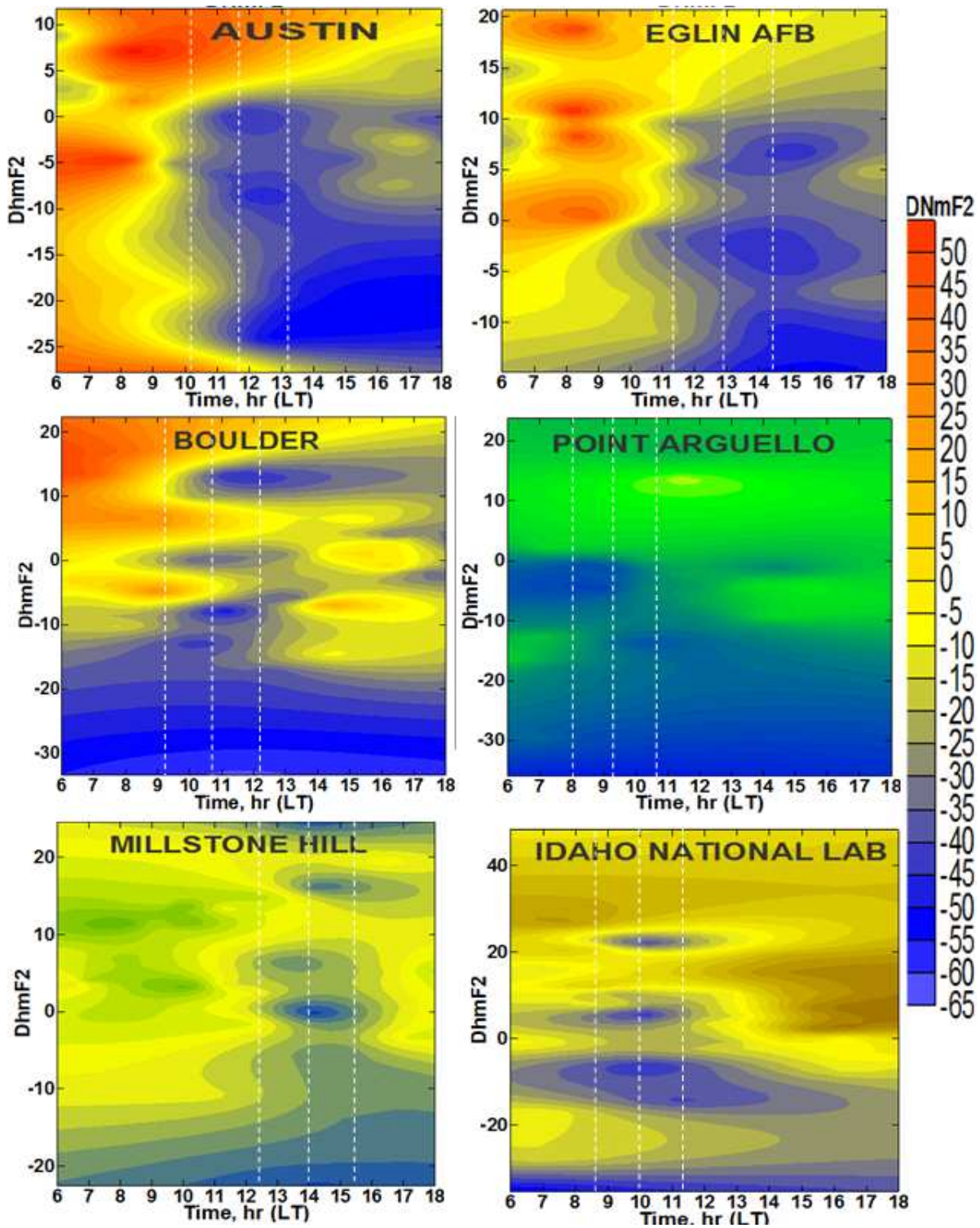


441

442

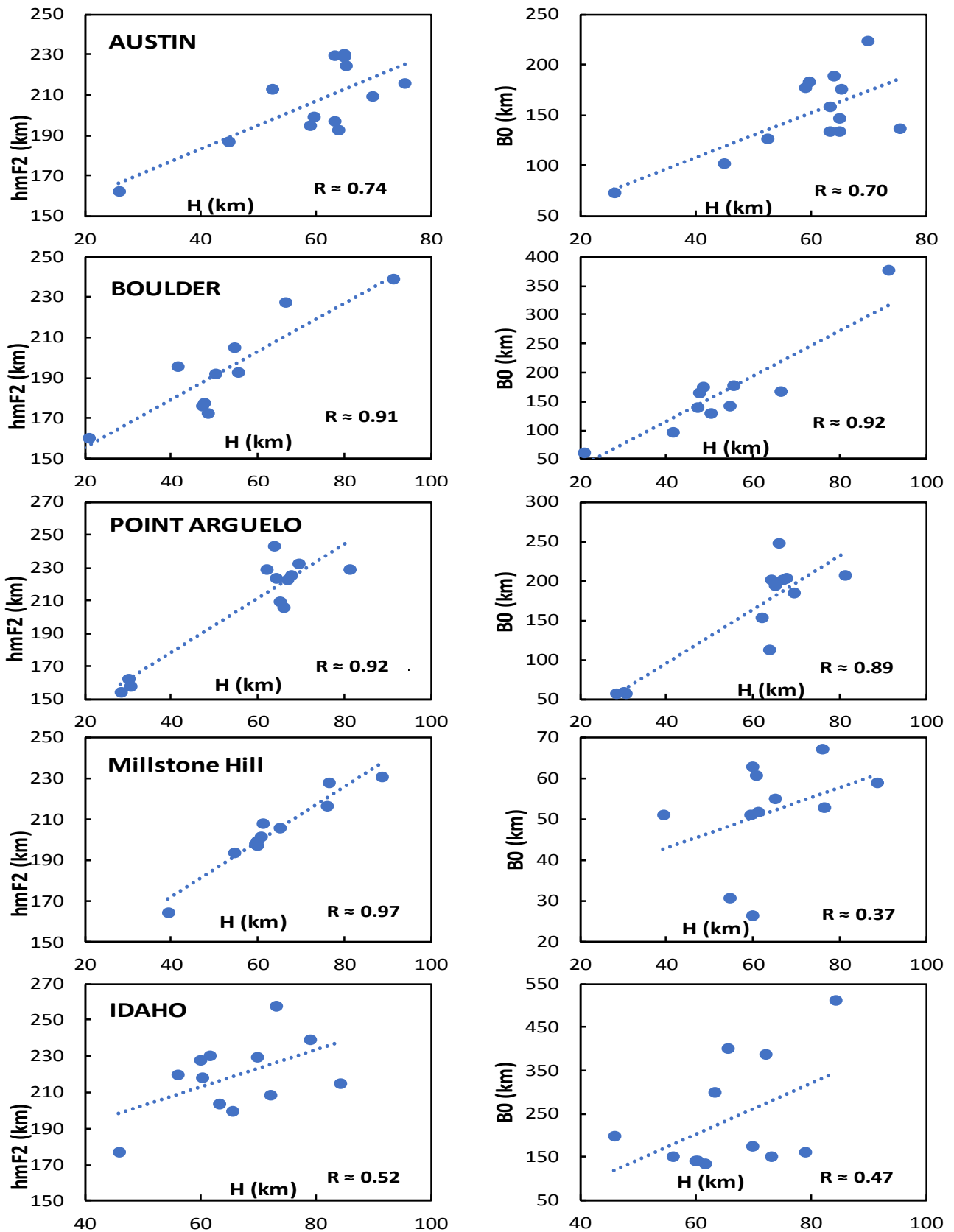
443

**Figure 2:** The local time variation of the ionospheric scale height and the bottomside ( $BO$  and  $B1$ ). The other features are the same as in Fig. 1.



444

445 **Figure 3:** Variation of the percentage deviation of  $NmF2$  ( $DNmF2$ ) and  $hmF2$  ( $DhmF2$ ) magnitudes for  
 446 observing the changes in the behaviour of the thermospheric composition and wind flow related to the loss  
 447 rate during the eclipse phase in comparing to the period before/after the event. The three vertical dashed  
 448 lines marked the eclipse start time, the time of maximum obscuration and the last contact time of the  
 449 eclipse (i.e. eclipse phase). The direction of wind was identify using the  $DNmF2$  colour legend, the negative  
 450 values represents the westward wind direction and the positive values is for the eastward wind.



451  
452  
453

**Figure 4:** Linear relationship of H versus *hmF2* and H versus *BO* during the eclipse of 21 August 2017 progression phase.